Supplementary Information

A Mechanical-assisted Post-bioprinting Strategy for Challenging Bone Defects Repair

Jirong Yang[1,2], Zhigang Chen[1,2], Chongjian Gao[1], Juan Liu[1], Kaizheng Liu[1], Xiao Wang[3], Xiaoling Pan[3], Guocheng Wang[1,2], Hongxun Sang[3], Haobo Pan[1,2], Wenguang Liu[4], Changshun Ruan[1,2,]*

[1] Research Center for Human Tissue and Organs Degeneration, Institute of Biomedicine and Biotechnology, Shenzhen Institute of Advanced Technology, Chinese Academy of Sciences, Shenzhen 518055, China

[2] University of Chinese Academy of Sciences, Beijing 100049, China

[3] Shenzhen Hospital, Southern Medical University, Shenzhen 518000, PR China

[4] School of Materials Science and Engineering, Tianjin Key Laboratory of Composite and Functional Materials, Tianjin University, Tianjin 300350, China

*Corresponding author (E-mail: cs.ruan@siat.ac.cn)

Supplementary Methods

Rheological test of GLN hybrid inks

The rheological properties of GLN hybrid inks were conducted using a shear rheometer (MCR 302, Anton Paar, Austria). To assess shear thinning properties, viscosity was measured as a function of shear rate 0.1 to 10 s^{-1} at 25 °C. Shear recovery was assessed by applying shear rate sweeps at three stages with shear rate 0.1 s^{-1} (60 s) - 1 or 10 or 50 s^{-1} (5 s) - 0.1 s^{-1} (60 s), T = 25 ºC. Strain-yielding behavior was assessed using a strain sweeps test, and the shear strain was changed successively from strain 1% (90 s) to strain 50%, 100%, 150% (90 s), with f = 1 Hz and T = 25 ºC.

Characterization of GLN hydrogels

Morphology observation. The GLN hydrogels were sharply frozen in liquid nitrogen and lyophilized immediately. The cross sections of the freeze-dried samples (n = 3) were observed under a field emission scanning electron microscopy (SEM, Hitachi S-4800, Japan). In addition, the elemental analysis (Si and Mg) of the GLN hydrogels were detected using an energy dispersive spectrophotometer (EDS, Hitachi, Japan).

Mechanical properties. All the GLN hydrogels were immersed in PBS to reach swelling equilibrium before the test. The compression modulus and strength of GLN hydrogels (φ 8 mm × h 10 mm, n = 4) were determined using a mechanical analyzer (Care, IBTC-300SL, China) at room temperature and the crosshead speed at 0.05 mm/s. The modulus of GLN hydrogels was obtained by the initial (straight line) linear slope of the stress-strain curve. The compressive strength was the peak of stress from the stress-strain curve. The stress relaxation was measured under 20% strain, and the relaxation time was defined as the time that the stress reduces to half of the initial stress.

Water absorption. The water adsorption of GLN hydrogels was measured by incubating the hydrogels (φ 10 mm × h 0.5 mm, n = 4) in PBS at 37 ºC for 12 h to reach swelling equilibrium. Wet weight (W) was recorded at preset time points. The rate of water adsorption was defined as $(W-W_0)/W_0 \times 100\%$, where W_0 was the initial wet weight of the samples. Besides, the gross morphology was imaged with a digital camera.

Water contact angles test. The water contact angle of the GLN hydrogels was examined with an automatic video micro contact angle-measuring instrument. The deionized water falling on top surfaces of samples (n = 4) had a volume of 5μL and a velocity of 1μL s^{-1}, then images of droplets were recorded by microscope lens and a camera. Analysis and processing software was used to calculate the contact angle of the GLN hydrogels.

Cell viability, spreading, proliferation and osteogenic differentiation of cells on GLN hydrogels

Cell culture. Human bone marrow mesenchymal stem cells (hBMSCs) (Cyagen, HUXMF-01001, Guangzhou) were cultured in a-MEM containing 10% fetal bovine serum (FBS, Gibco) and 100 U/mL penicillin/streptomycin in a humidified atmosphere with 5% CO_2 at 37 ºC. hBMSCs at passage 6 (P6) were used for further experiments. The hBMSCs were seeded onto the sterilized GLN hydrogels (φ 10 mm × h 0.5 mm) placed in 24-well cell culture plates (Corning) at a seeding density of 2×10^4 cells/well.

Cell viability. Live/dead viability was used for determining cell viability. The samples cultured for 1 day were stained with 5 μg/mL fluorescein diacetate (FDA, Sigma) and 5 μg/ml propidium iodide (PI, Sigma), after washing the samples with PBS, cell viability in the hydrogels was observed visually with a confocal laser scanning microscopy (CLSM, Leica SP8, Germany).

Cell adhesion and spreading. The samples cultured for 1 day were fixed in 4% paraformaldehyde for 10 min at 4 °C. After cell permeabilization and blocking with 0.1% Triton-X and 10% goat serum, respectively. Then, the samples were incubated with an anti-vinculin antibody (Abcam, ab129002) at 1:100 dilution in 1% BSA-containing PBS solution at 4 °C overnight. Subsequently, the samples were washed 5 times by flowing PBS and treated with the goat anti-rabbit IgG Alexa Fluor 488 conjugate secondary antibody (Abcam, ab150077) at 1:500 dilution for 1 h at room temperature. Meanwhile, to visualize cell spreading, the samples were incubated in 5 U/mL Alexa Fluor-594 phalloidin (Invitrogen, A12381) for 45 min at room temperature, and cell nuclei were stained with Hoechst 33342. Finally, the stained samples were examined under a CLSM.

Cell proliferation. For quantitative analysis of cell proliferation, the samples were incubated in a serum-free medium containing 10% CCK8 (Dojindo, Japan) and measured using a multi-detection microplate reader (Bio-Rad 550). Cell proliferation was analyzed on 1, 3, and 5 days.

Alkaline phosphatase (ALP) staining. The activity of alkaline phosphatase was detected with a BCIP/NBT staining kit (Beyotime, C3206) according to the manufacturer's protocol. Briefly, the samples cultured for 7 days were fixed in 4% paraformaldehyde for 10 min at 4 °C and incubated with BCIP/NBT working solution at 4 °C overnight. Then, the samples were washed 3 times with deionized water. The images were acquired by an optical microscope.

Immunofluorescence staining. The samples cultured for 14 days were harvested for detecting collagen I (Col I). Immunofluorescence staining was performed as described above. The primary antibody and secondary antibody were anti-Col I at dilution 1:200 (Abcam, ab34710) and goat anti-rabbit IgG Alexa Fluor 488 at 1:500 dilution (Abcam, ab150077), respectively.

qRT-PCR. Osteogenic gene expression (ALP and COLI) was assessed by qRT-PCR. At 7 days, the samples (n = 3) were collected. Total RNA was extracted according to the manufacturer's instructions for the RNeasy

Mini Kit (Qiagen, 74904). And then, the extracted RNA was reverse-transcribed into cDNA using the RevertAid First Strand cDNA Synthesis Kit (Invitrogen, K1622). Quantitative real-time PCR was performed using the CFX96TM real-time PCR detection system (Bio-Rad, USA) with RealStar Fast SYBR qPCR Mix (Genstar, A301). The cycling conditions for qRT-PCR are 95 °C for 2 min, followed by 40 cycles of 95 °C for 15 s, 60 °C for 15 s, and 72 °C for 30 s. And the gene expression level of each targeted gene was determined by the △△Ct method, and GAPDH was used as a housekeeping gene to normalize the results. The sequences of the primers are given in Supplementary Table 2.

The rat subcutaneous implantation and repair of distal femoral metaphyseal defect

To assess the hollow structures of HHSs in promoting blood vessel growth and bone formation, two groups of HHSs ($L_{0.4}D_{0.6}d_0$ and $L_{0.4}D_{0.6}d_{0.4}$) were used. Subcutaneous implantation and a distal femoral metaphyseal defect model were established. All animals were 3 months old in the experiments. The animal experiments were approved by the Institutional Animal Care and Use Committee of Shenzhen Institute of Advanced Technology, Chinese Academy of Science.

For subcutaneous implantation, two subcutaneous pockets for implantation of the HHSs (length 8 mm, width 8 mm, height 4 mm) were made on the backs of rats under aseptic and anesthetic conditions. Two groups were respectively transplanted into the left and right (n = 4 for each group). The skin was closed with interrupted sutures. After 2 weeks of surgery, animals were sacrificed, and all specimens were collected, fixed in 4% paraformaldehyde, embedded in paraffin, sectioned at 5 μm thickness, and stained with H&E.

The surgical procedure for distal femoral metaphyseal defect was the same as the rat osteoporotic bone defect model. A distal femoral metaphyseal critical-size defect (φ 3 mm × h 4 mm) was established in normal rats. Two groups were respectively transplanted into the left and right of the rat's defects at random (n = 3 for each group). All samples used here were designed as a cylinder (φ 3 mm × h 4 mm). After 8 weeks of surgery, all animals were sacrificed and the distal femurs for each group were collected, and fixed in 4% paraformaldehyde for 48 h. all samples were scanned using a μCT, then decalcified with EDTA, embedded in paraffin, sectioned at 5 μm thickness, and processed according to standard histological staining procedures. The sections were stained with H&E and Masson's trichrome

Isolation, verification of senescence and osteogenic differentiation of OVX-BMSCs

BMSCs and OVX-BMSCs were respectively isolated from long bones of limbs of healthy and osteogenic rats. Then, alpha-modified Eagle's medium (α-MEM, HyClone) containing 20% fetal bovine serum (FBS, Gibco) and 100 U/mL penicillin/streptomycin (Hyclone) was injected using syringes to flush cells out of marrow

cavities. The cells were cultured in a humidified atmosphere with 5% CO2 at 37 °C. After 24 hours, the medium was replaced with fresh culture medium to remove nonadherent cells. The cells were sub-cultured in α-MEM containing 10% FBS and 100 U/mL penicillin/streptomycin until passage 2 (P2). The P2 cells were then harvested for further study. BMSCs and OVX-BMSCs were respectively seeded on the 24-well plates at a cell density of 2×10^4/well. Cell senescence was assessed by the senescence β-galactosidase (SA-βgal) staining kit (Beyotime) and qRT-PCR for p16 gene expression. Cell proliferation was analyzed on 1 and 3 days by CCK8. In addition, the ability of osteogenic differentiation was evaluated by ALP staining on 4 and 7 days and alizarin red (ARS) staining on 14 and 21 days, and qRT-PCR for *Runx2*, *Alp*, *Bmp2*, *Bsp*, *Col 1a1* and *Ocn* genes expression on 7 days.

Supplementary Figs

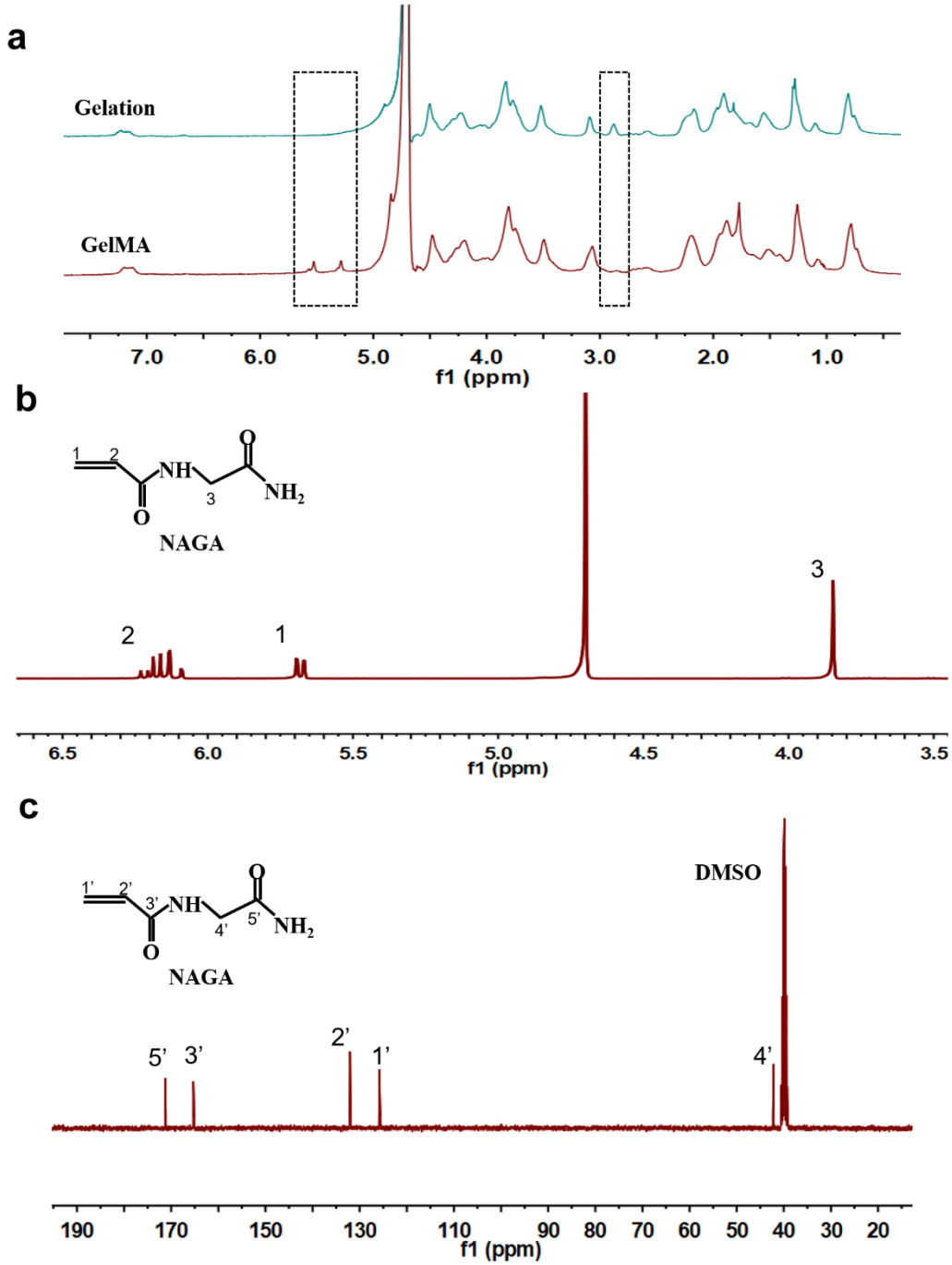

Supplementary Fig. 1 Characterization of the synthesized GelMA and NAGA. a, ^{1}H NMR spectrum of synthesized GelMA in D_2O. Two distinctive peaks at about δ 5.6 ppm and δ 5.4 that were attributed to the protons of double bond (C = CH_2) appeared, indicating successful grafting of MA in gelatin. The quantitative analysis of the ^{1}H NMR spectrum shows that the degree of methacrylate of gelatin was 67 ± 2%. **b**, ^{1}H NMR spectrum of NAGA in D_2O. **c**, ^{13}C NMR spectrum of NAGA in DMSO-d_6.

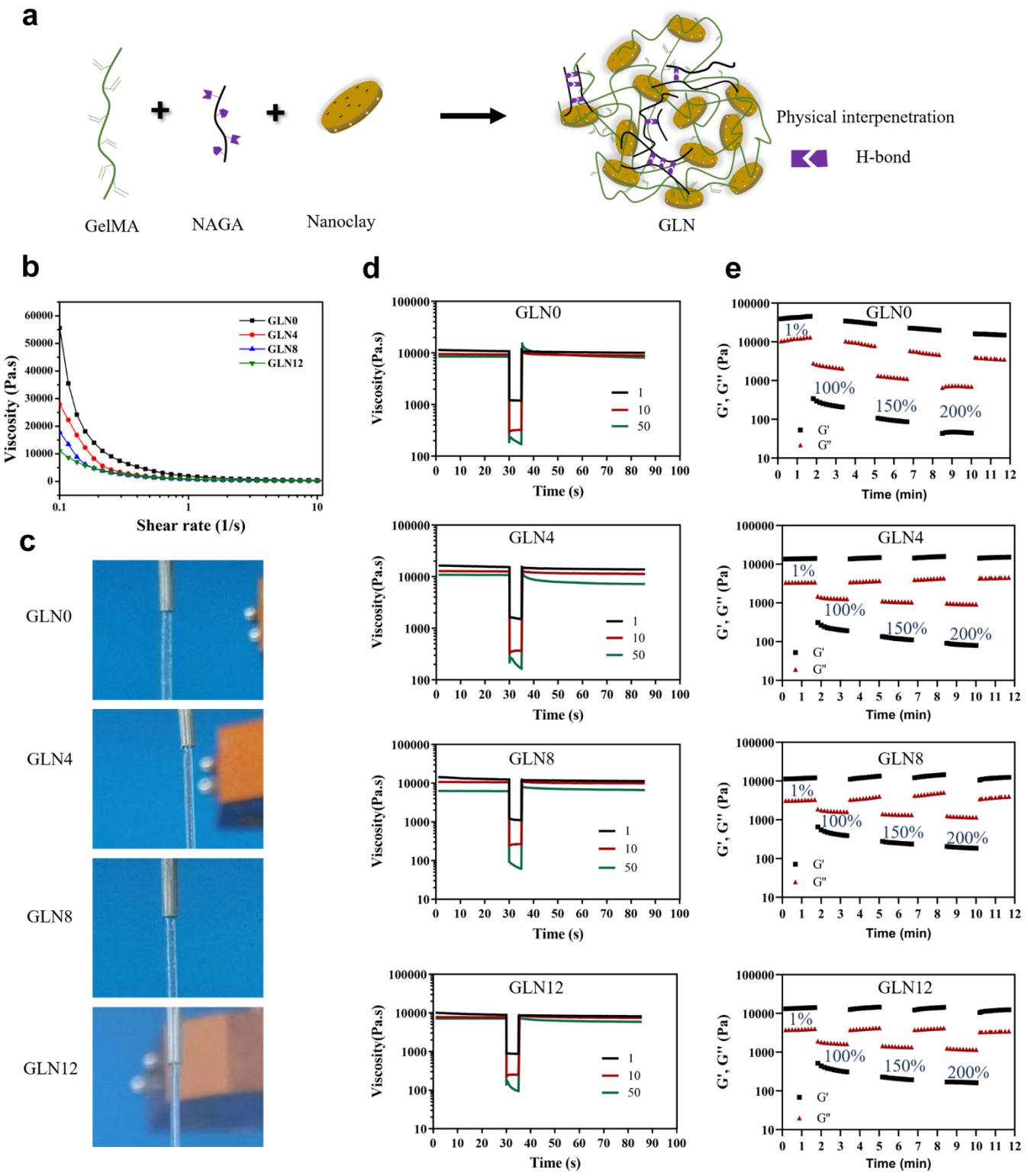

Supplementary Fig. 2 Rheological properties of GLN hybrid inks. a, The schematic diagram of the physical interpenetration of GLN hybrid inks. **b**, Viscosity of hybrid GLN inks in a shear rate sweep from 0.1 to 10 s^{-1} at 25 °C. **c**, Photographs of extruded hollow filaments via a coaxial nozzle using GLN hybrid inks without supporting materials. **d**, Viscosity of GLN hybrid inks in shear rate sweeps at three stages with shear rate 0.1 s^{-1} (60 s) - 1 or 10 or 50 s^{-1} (5 s) - 0.1 s^{-1} (60 s) at 25 ºC. **e**, Storage modulus (G') and loss modulus (G'') of GLN hybrid inks in shear strain sweeps from successively strain 1% (90 s) to strain 50%, 100%, 150% (90 s), with f = 1 Hz and T = 25 ºC.

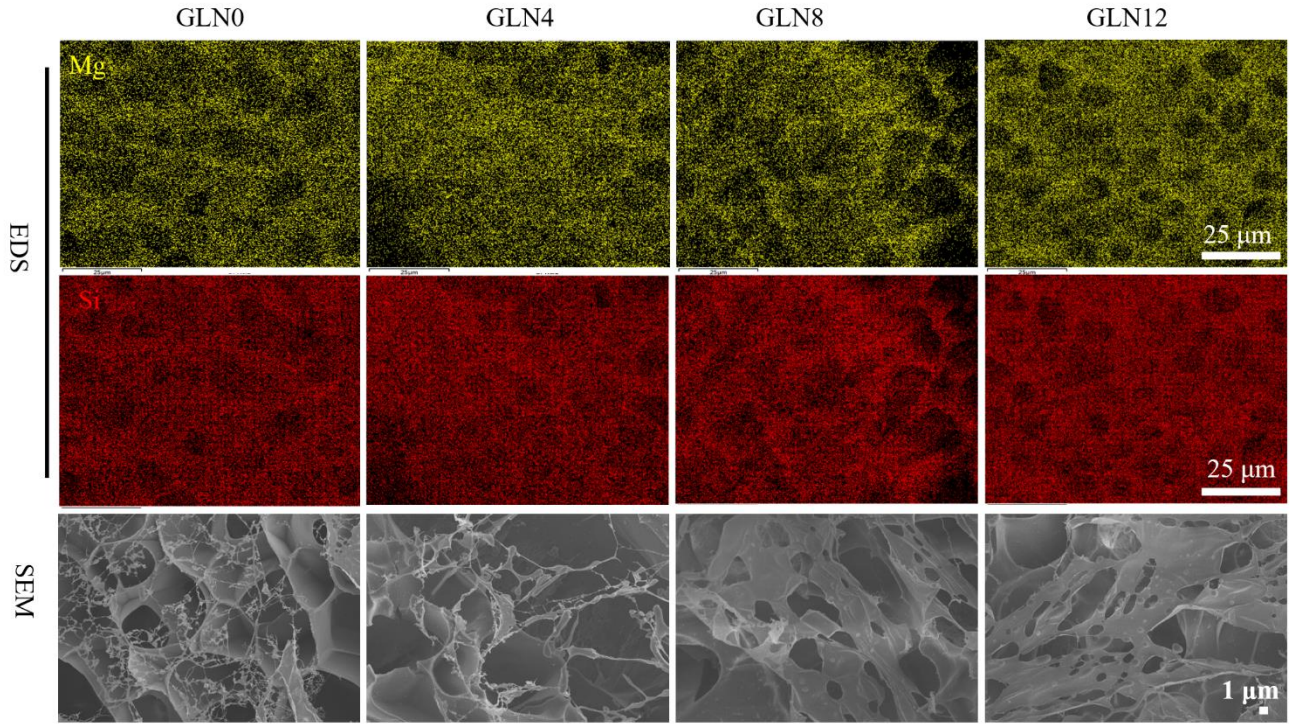

Supplementary Fig. 3 Microscopic morphology observation (EDS and SEM) of GLN hydrogels.

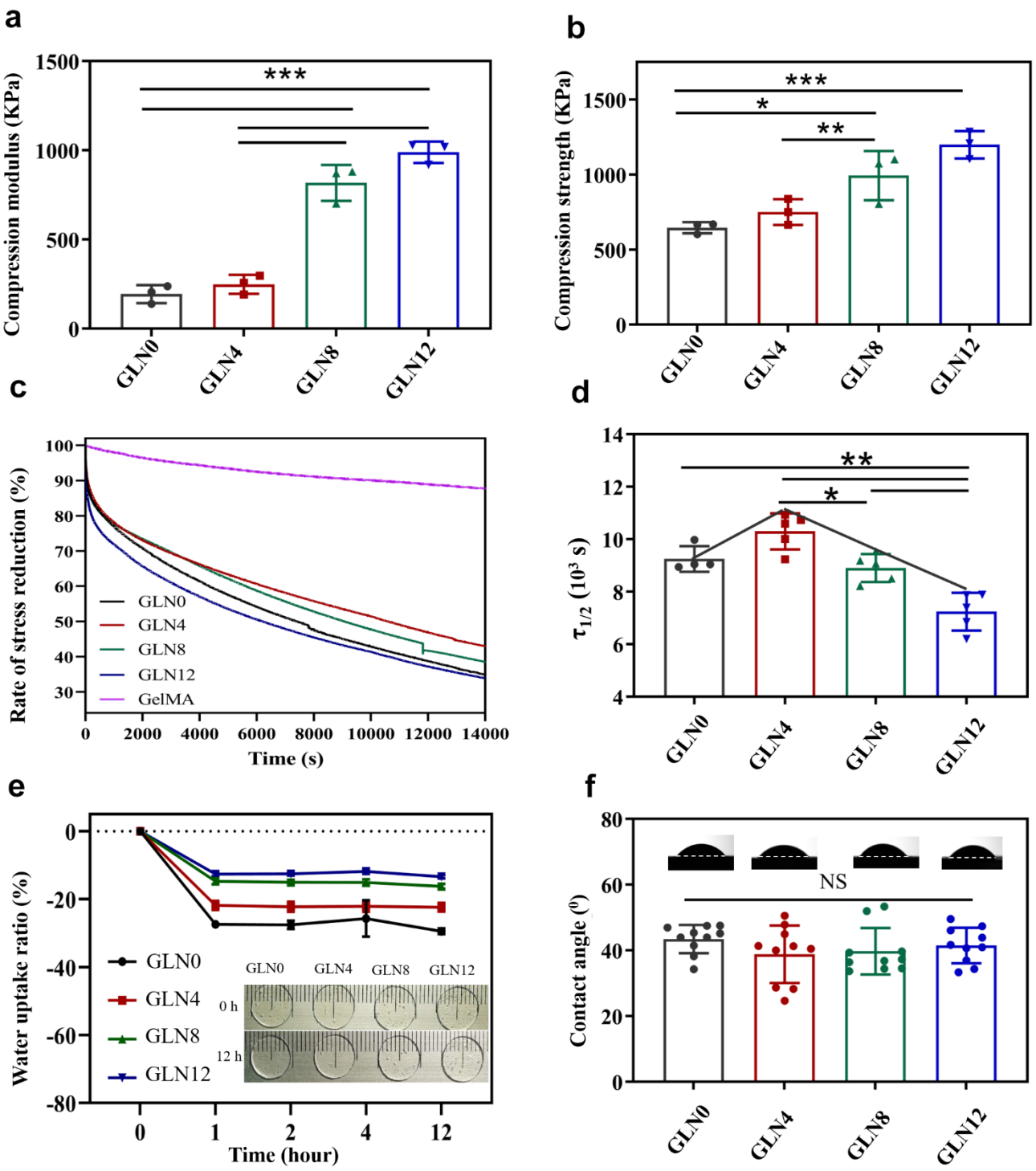

Supplementary Fig. 4 Physical properties of GLN hydrogels. a,**b**, Compression modulus (**a**) and compression strength (**b**) of GLN hydrogels. **c**,**d**, The curve of stress relaxation (**c**) and relaxation time (**d**) defined as the time that the stress reduces to half of the initial stress under 20% strain. **e**, Water uptake of GLN hydrogels in PBS at 37 ºC for 12 h. **f**, Water contact angle of GLN hydrogels. Dates are presented as means ± s.d, n = 4 per group, statistical significance was calculated using Tukey's multiple comparisons tests, *P < 0.05, **P < 0.01, ***P < 0.001, NS represents no significant difference.

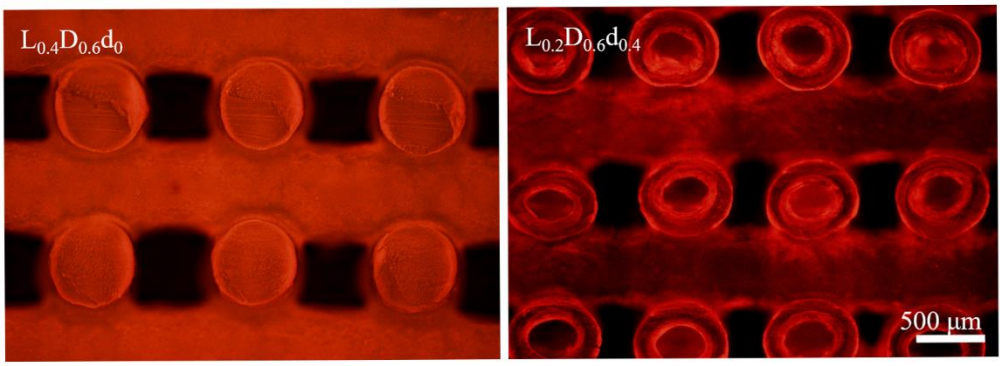

Supplementary Fig. 5 The fluorescent images of hollow structures of $L_{0.4}D_{0.6}d_0$ and $L_{0.2}D_{0.6}d_{0.4}$ HHSs.

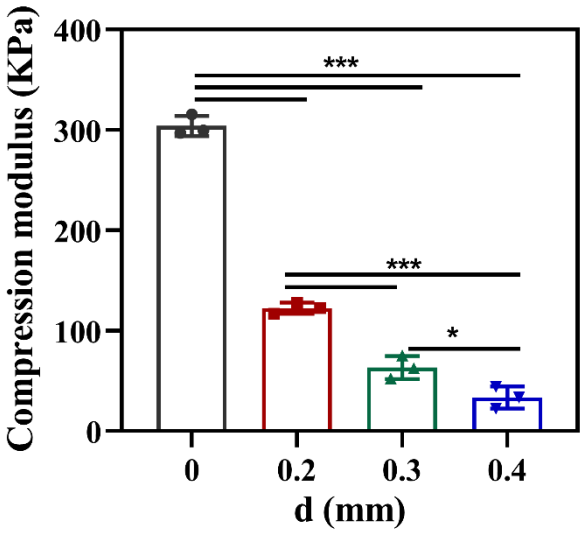

Supplementary Fig. 6 The compression modulus of the $L_{0.4}D_{0.6}d_z$ (z = 0, 0.2, 0.3, and 0.4) HHSs. Dates are presented as means ± s.d, n = 4 per group, statistical significance was calculated using Tukey's multiple comparisons tests, *P < 0.05, ***P < 0.001.

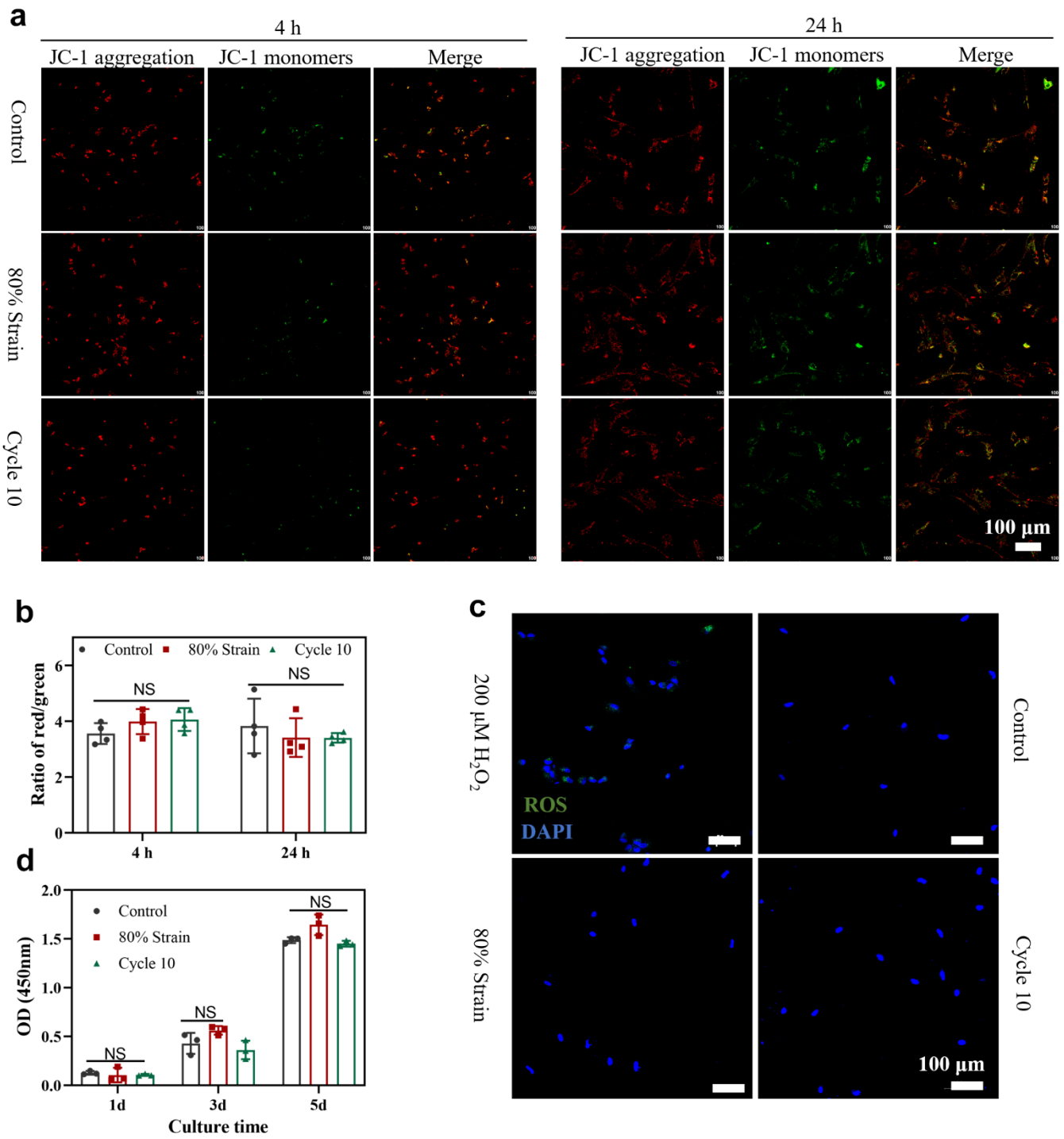

Supplementary Fig. 7 Cell viability after mechanical stimulation with 80% strain and 10 cycles of compression-recovery under 40% strain. a,**b**, The fluorescence images (**a**) and quantitative analysis of the fluorescent intensity of red/green ratio (**b**) of cells stained by JC-1 after undergoing mechanical stimulation for 4 h and 24 h of culture, JC-1 aggregation (red) and JC-1 monomers (green) of cells, the cells that did not undergo mechanical stimulation were as a control group. **c**, Fluorescence images of ROS generated by cells via a probe DCFH-DA after undergoing mechanical stimulation for 4 h of culture, the cells cultured with 200 μM H_2O_2 were as a positive group. **d**, CCK8 assay of the cells undergoing mechanical stimulation for 1, 3, and 5 days of culture. Dates are presented as means ±s.d, n = 4 per group, statistical significance was calculated using Tukey's multiple comparisons tests, and NS represents no significant difference.

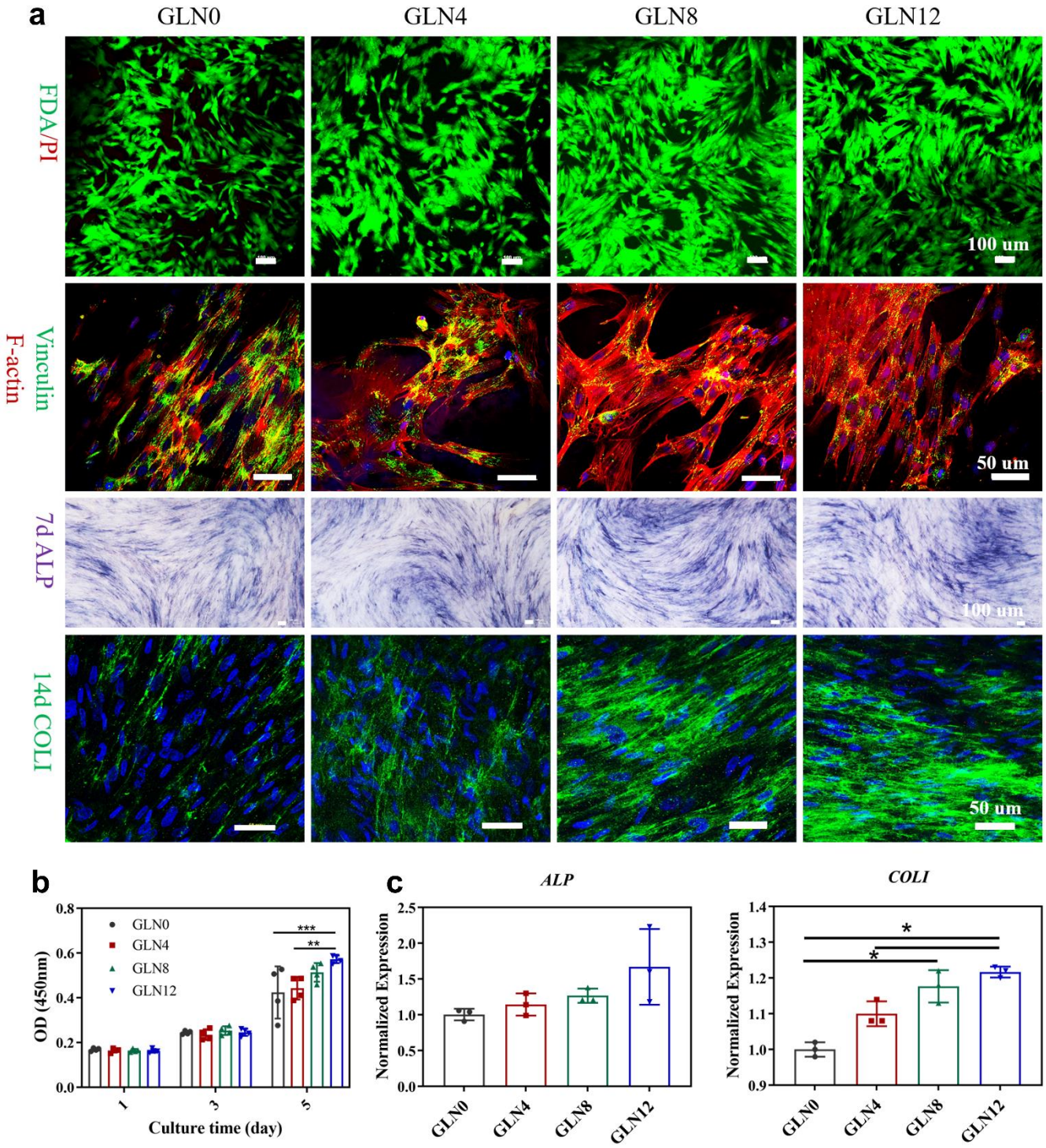

Supplementary Fig. 8 The viability, spreading, proliferation, and osteogenic differentiation of hBMSCs on GLN hydrogels. a, Live (green)/dead (red) staining by FDA and PI at 1 day, vinculin (green) and phalloidin (red) for F-actin at 1 day, ALP staining at 7 days and immunofluorescence staining of Col I at 14 days. **b**, CCK8 assay for quantitative analysis of hBMSCs proliferation on GLN hydrogels at 1, 3, and 5 days. **c**, Genes expression of ALP and COLI of hBMSCs on GLN hydrogels at 7 days. Dates are presented as means ± s.d, n = 3 per group, statistical significance was calculated using Tukey's multiple comparisons tests, *P < 0.05, **P < 0.01, ***P < 0.001.

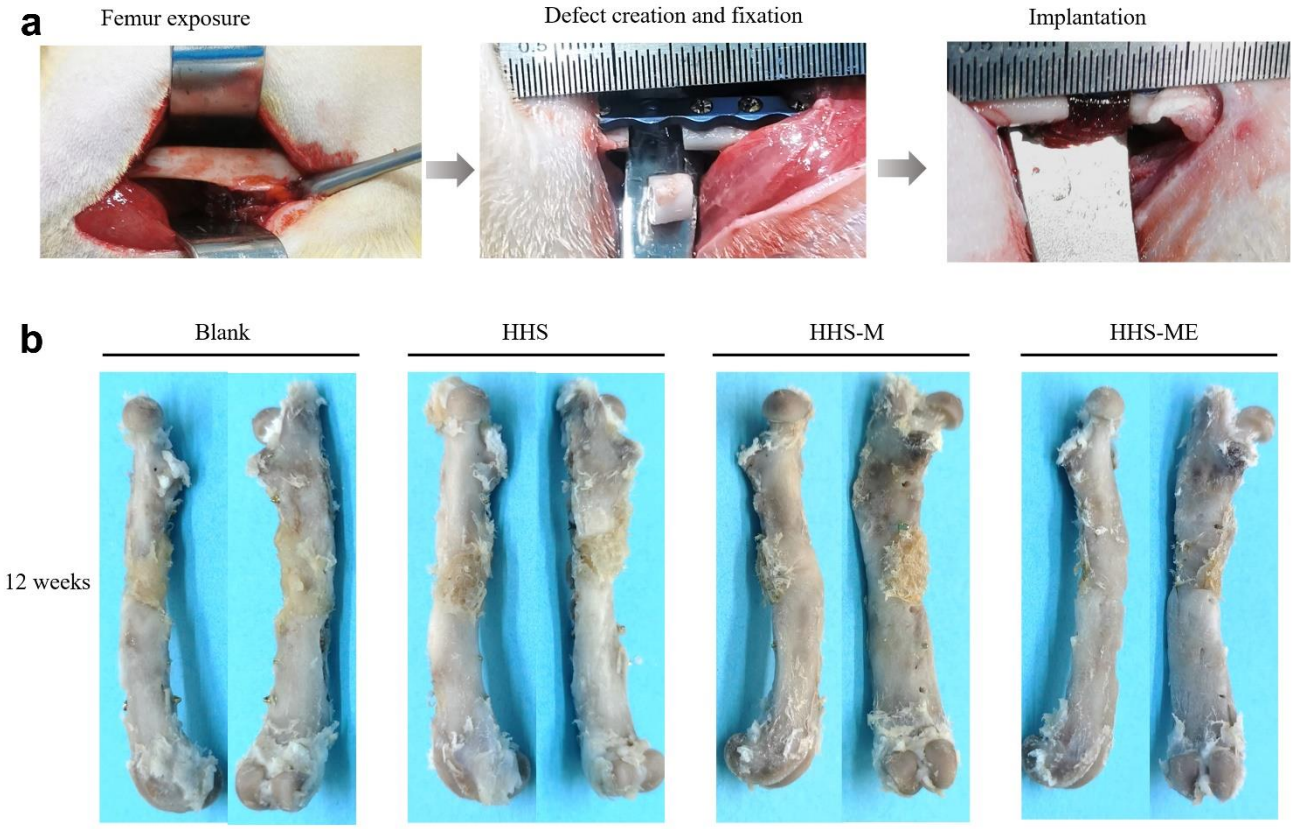

Supplementary Fig. 9 The bone regeneration of the large-size segmental bone defects by the HHS-cells (HHS-M and HHS-ME). a, Photographs of the surgical process. **b**, Photographs of gross view of the femurs of rats with 5-mm critical femoral mid-diaphyseal defects at 12 weeks after surgery, the defects were treated with four groups (Blank, HHS, HHS-M, and HHS-ME) respectively.

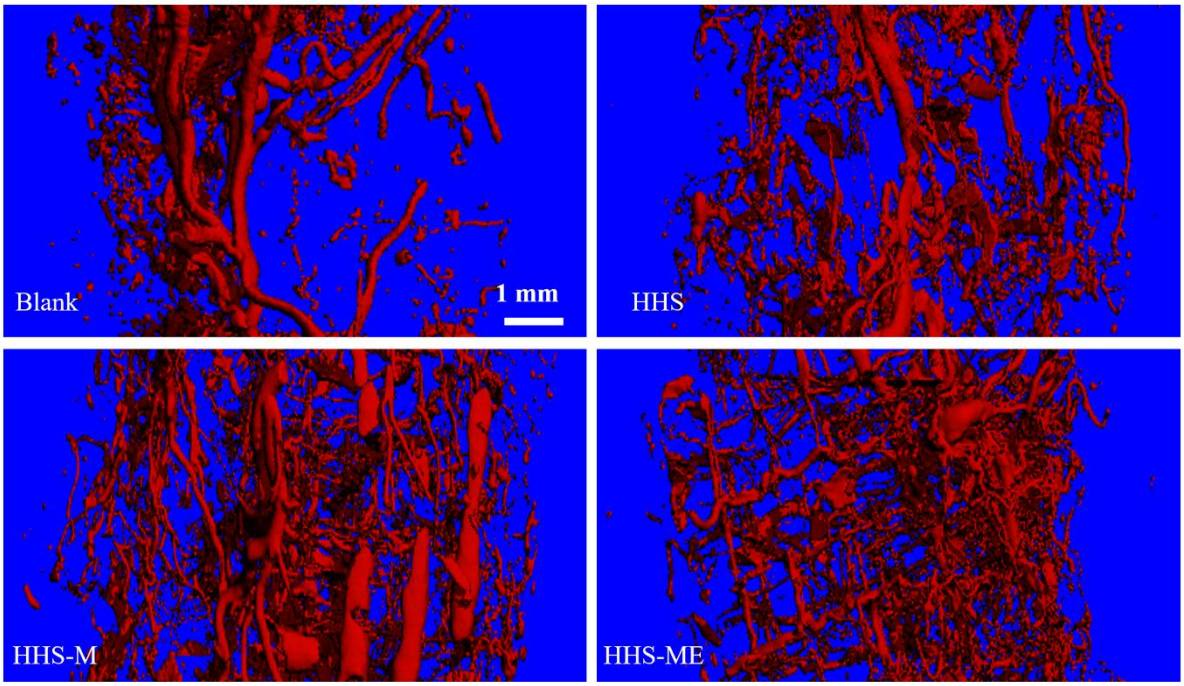

Supplementary Fig. 10 The reconstruction of blood vessels in large-sized segmental bone defects of Blank, HHS, HHS-M, and HHS-ME group at 6 weeks after surgery.

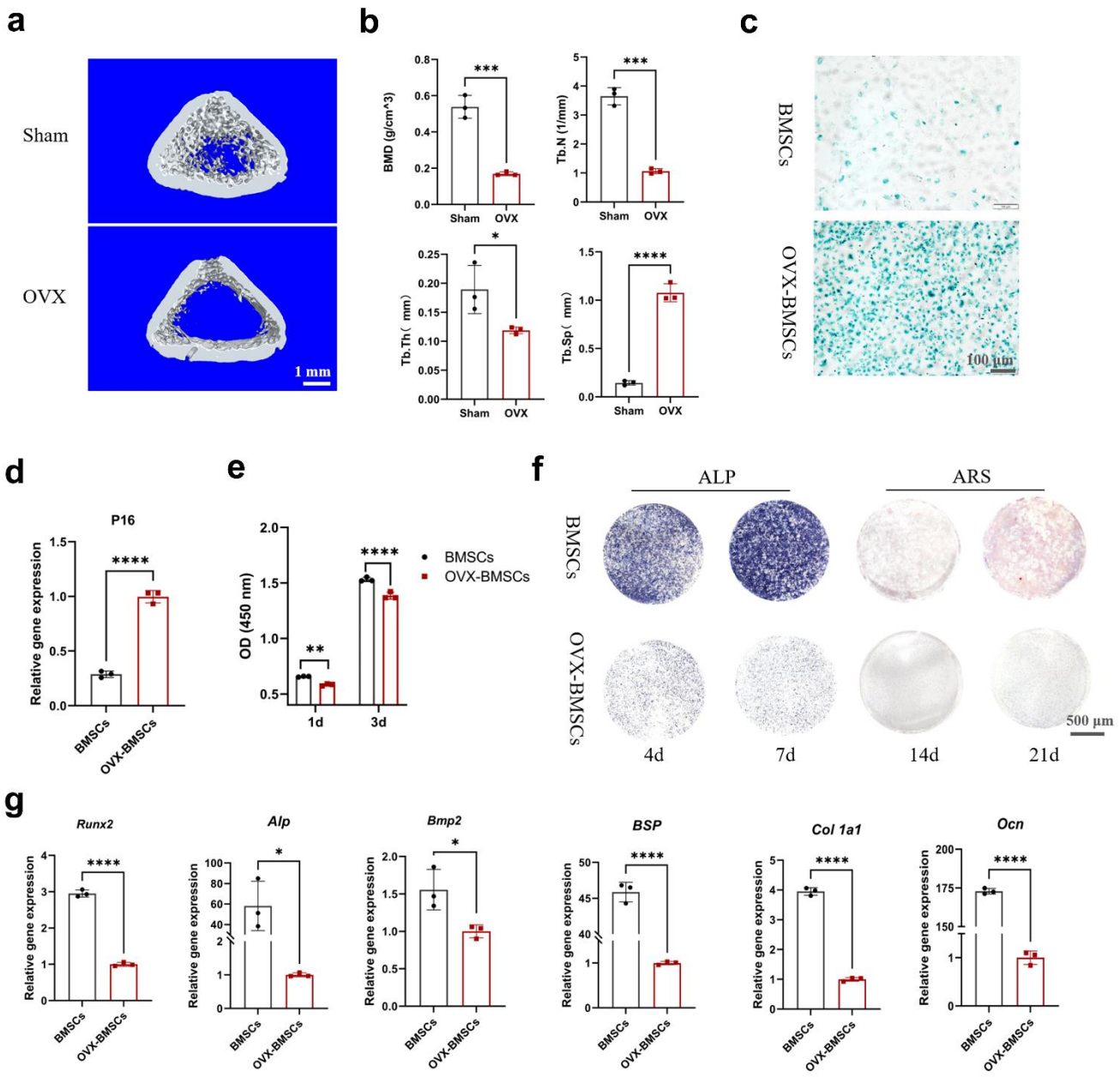

Supplementary Fig. 11 Osteoporotic rat models, senescence and osteogenic differentiation of OVX-BMSCs. a, μCT reconstruction images showing cross-section views of sham and ovariectomized groups at week 12 after surgery. **b**, Quantitative analysis of bone mineral density (BMD), bone trabeculae number (Tb.N), bone trabecular thickness (Tb.Th) and trabecular separation (Tb.Sp) from the reconstructed μCT images. **c,d,e,** SA-βgal staining (**c**), Gene expression of *P16* (**d**) and CCK8 assay (**e**) of BMSCs and OVX-BMSCs. **f**, ALP staining at day 4 and 7, and ARS staining at day 14 and 21. **g**, Gene expression of *Runx2*, *Alp*, *Bmp2*, *Bsp*, *Col 1a1* and Ocn on 7 days. Dates are presented as means ± s.d, n = 3 per group, statistical significance was calculated using Tukey's multiple comparisons tests, *P < 0.05, **P < 0.01, ***P < 0.001.

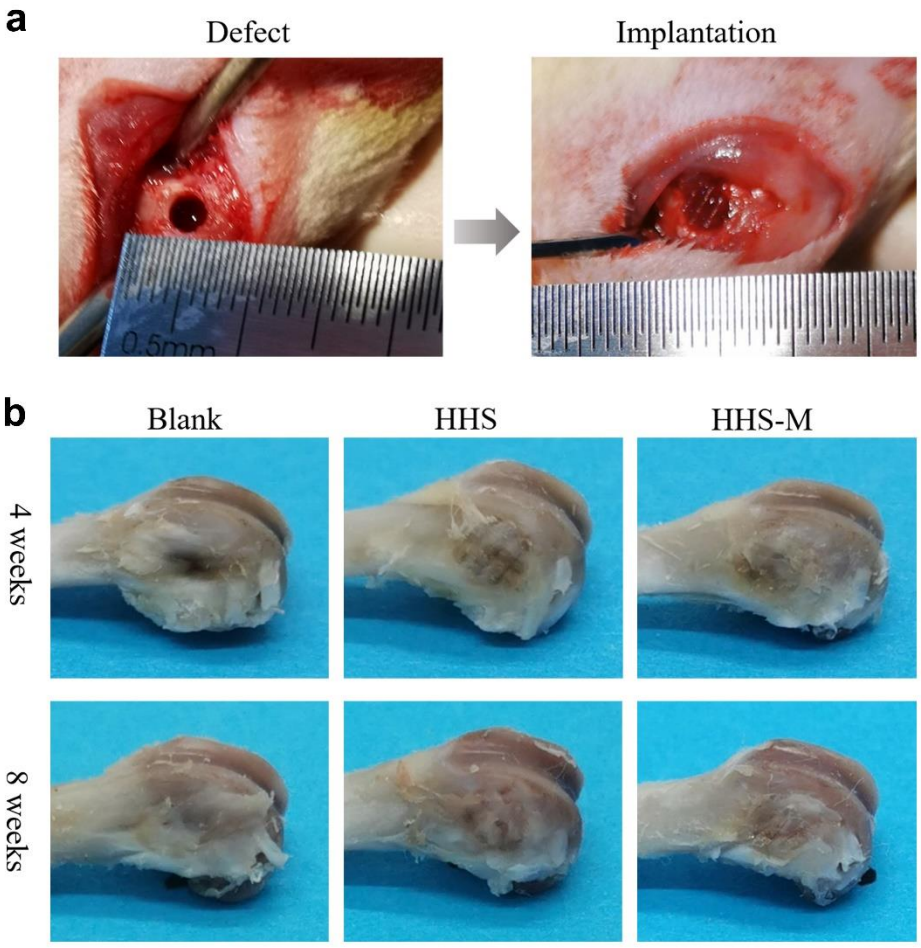

Supplementary Fig. 12 The bone regeneration of osteoporotic bone defects by the HHS-cells (HHS-M). a, Photographs of the surgical process. **b**, Photographs of the gross view of distal femurs of rats with critical defects (φ3 mm × h 4 mm) at 4 and 8 weeks after surgery, the defects were treated with three groups (Blank, HHS, and HHS-M) respectively.

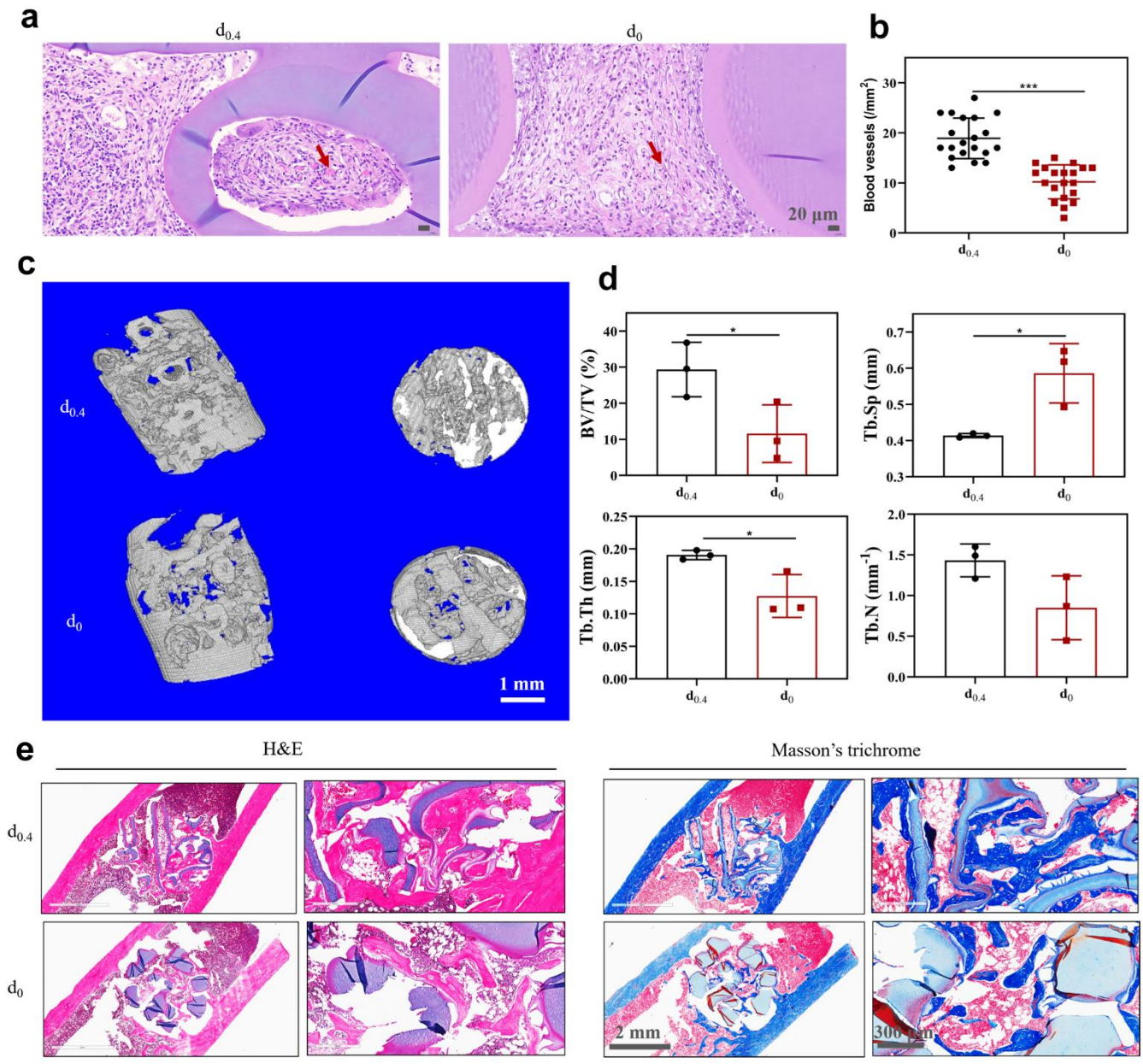

Supplementary Fig. 13 The rat subcutaneous implantation and repair of distal femoral metaphyseal defects to evaluate the effect of hollow structure of HHS$_S$ ($L_{0.4}D_{0.6}d_0$ and $L_{0.4}D_{0.6}d_{0.4}$) on blood vessels ingrowth and bone formation. a, H&E staining of the subcutaneous implantation samples at 2 weeks, red arrows represent blood vessels that grew in the HHSs after surgery. **b**, Quantitative analysis of the blood vessels that grew in the HHSs according to the H&E staining. n = 4 rats per group, 5 images for each sample. Dates are presented as means ± s.d, statistical significance was calculated using Student's t-tests, ***P < 0.001. **c**, μCT reconstruction images of new bone view of metaphyseal bone in the defective region at 8 weeks after surgery. **d**, Quantitative analysis of bone volume to the total defect volume (BV/TV), bone trabeculae number (Tb.N), trabecular separation (Tb.Sp), and trabecular thickness (Tb.Th) from the reconstructed μCT images at 8 weeks. Dates are presented as means ± s.d, statistical significance was calculated using Student's t-tests, n = 3 rats per group. *P < 0.05. **e**, H&E and Masson's trichrome staining at 8 weeks, obviously new bone formation in the d_0 HHS group.

Supplementary Tables

Supplementary Table 1. The ratio of theoretical volume of V_1 and V_2 to the total volume of HHSs and water uptake ratio of HHSs in static condition

Group	Ratio of volume of V_1 (%)	Ratio of volume of V_2 (%)	Water uptake ratio (%)
$L_{0.4}D_{0.6}d_{0.4}$	22.1±3.3	39.2±5.8	33.7±1.4
$L_{0.4}D_{0.6}d_{0.3}$	12.7±1.9	39.2±5.8	38.3±1.8
$L_{0.4}D_{0.6}d_{0.2}$	5.7±1.0	39.2±5.8	34.4±3.7
$L_{0.4}D_{0.6}d_{0}$	0	39.2±5.8	37.9±2.8
$L_{0.2}D_{0.6}d_{0.4}$	28.7±2.5	27.7±5.4	27.6±0.5
$L_{0.6}D_{0.6}d_{0.4}$	18.3±2.8	49.0±4.3	49.0±0.5

Supplementary Table 2. The forward and reverse primer sequences for qRT-PCR

Gene	Forward primer sequences (5'-3')	Reverse primer sequence (5'-3')
GAPDH	TCAAGGCTGAGAACGGGAA	TGGGTGGCAGTGATGGCA
ALP	TTGACCTCCTCGGAAGACACTC	CGCCTGGTAGTTGTTGTGAGC
Col I	CACACGTCTCGGTCATGGTA	AAGAGGAAGGCCAAGTCGAG

Supplementary Videos

Supplementary Video 1 Actual process of printing bone-shaped construct

Supplementary Video 2 Compression tests of HHSs with 80% stain

Supplementary Video 3 Visual process of compression-recovery of HHSs

Supplementary Video 4 Processes of two cell seeding approaches: direct cell seeding and cell seeding by V_2-mechanical response